



OPEN

SUBJECT AREAS:
THERMODYNAMICS
BIOLOGICAL PHYSICSReceived
28 May 2014Accepted
12 September 2014Published
3 November 2014Correspondence and
requests for materials
should be addressed to
V.A.P. (parsegian@
physics.umass.edu)

Continuity of states between the cholesteric \rightarrow line hexatic transition and the condensation transition in DNA solutions

Selcuk Yasar¹, Rudolf Podgornik^{1,2,3}, Jessica Valle-Orero^{4,5,6}, Mark R. Johnson⁷ & V. Adrian Parsegian¹

¹Department of Physics, University of Massachusetts, Amherst, MA 01003, United States, ²Department of Theoretical Physics, J. Stefan Institute, SI-1000 Ljubljana, Slovenia, ³Department of Physics, Faculty of Mathematics and Physics, University of Ljubljana, SI-1000 Ljubljana, Slovenia, ⁴Institut Laue Langevin, BP 156, 6, rue Jules Horowitz 38042 Grenoble Cedex 9, France, ⁵Laboratoire de Physique, Ecole Normale Supérieure de Lyon, 46 allée d'Italie, 69364 Lyon Cedex 07, France, ⁶Department of Biological Sciences, Columbia University, 1212 Amsterdam Avenue, New York, New York 10027, United States, ⁷Institut Laue-Langevin, 6 rue Jules Horowitz, BP156 38042, Grenoble, France.

A new method of finely temperature-tuning osmotic pressure allows one to identify the cholesteric \rightarrow line hexatic transition of oriented or unoriented long-fragment DNA bundles in monovalent salt solutions as first order, with a small but finite volume discontinuity. This transition is similar to the osmotic pressure-induced expanded \rightarrow condensed DNA transition in polyvalent salt solutions at small enough polyvalent salt concentrations. Therefore there exists a continuity of states between the two. This finding, together with the corresponding empirical equation of state, effectively relates the phase diagram of DNA solutions for monovalent salts to that for polyvalent salts and sheds some light on the complicated interactions between DNA molecules at high densities.

DNA at elevated osmotic pressures, accessible in highly concentrated DNA solutions *in vitro*, exhibits a sequence of ordered liquid-crystalline mesophases^{1–3} whose properties determine the nature of high density DNA compaction also in the biological milieu characterized by similar DNA densities, bathing solution conditions, and osmotic pressures. These biologically relevant examples of high density DNA compaction include most importantly DNA packing within virus capsids at osmotic pressures exceeding 60 atm and at densities within the regime of highly concentrated DNA solutions^{4–8}. Moreover, in eukaryotic sperm cells, DNA is packaged by a variety of simple basic proteins with positively charged polypeptide chains^{9–12} that condense DNA as condensing agents do in solution conditions^{13,14}. While the general outlines of the long-fragment (few microns long) DNA phase diagram seem to be properly characterized, with a well established progressive ordering sequence, isotropic \rightarrow cholesteric \rightarrow line hexatic \rightarrow orthorhombic phases, many details including the fragment length dependence¹⁵ remain to be systematically investigated.

In this paper, we concentrate on the question of the organization and packing of genomic length DNA chains and parameterization of the forces governing their interactions at biologically relevant DNA densities and osmotic pressures. The two most important DNA liquid-crystalline phases at these densities are the line hexatic¹ (LH) and the cholesteric¹⁶. The more ordered LH phase is observed at higher DNA densities, i.e., from approximately 300 mg/ml to 700 mg/ml, while the cholesteric phase then extends all the way to the isotropic phase, in which DNA is not ordered. In both the cholesteric and LH phases, DNA is locally oriented and positionally organized in a lattice with hexagonal bond orientational order¹⁷. However, while the bond orientational order in the cholesteric phase is short-range, it becomes *macroscopic* in the LH phase¹⁸, leading to the appearance of a sixfold azimuthally modulated x-ray diffraction intensity of the first-order diffraction peak when the chains are aligned parallel to the x-ray beam¹. Previous work could not definitively address the question whether this change in the nature of order is continuous or not.

While for long-fragment DNA the positional order in both phases remains liquid-like, the range of ordering changes quantitatively as the system is pushed through the transition between these two phases. In what follows, we present evidence that the range of the bond orientational order and the nature of the local positional ordering



change abruptly at the transition between these two phases, leading to a discontinuous jump in the DNA density and thus exhibiting the characteristics of a first-order transition. Furthermore, we note that the abrupt change in the radial widths of the first-order diffraction peaks, indicating the range of the positional order, occurs concurrently with the appearance of the sixfold azimuthal modulation of the first-order diffraction peak. A sharper well-defined peak seen in the LH phase indicates strong suppression of conformational fluctuations and the interaxial separation between the neighboring DNA chains changes discontinuously at the cholesteric \rightarrow LH transition, signaling a discontinuous change also in DNA density, controlled and varied by the osmotic stress of the bathing solution¹⁹. In order to observe this discontinuous change induced by the solution osmotic pressure, separating a first-order from a second-order transition between these two mesophases, a very precise means of controlling the DNA density is needed, implying also an accurate tuning of the osmotic pressure of the DNA solution. The latter is accomplished by fine temperature tuning of the bathing solution and its osmotic pressure, as described below.

We address two important unresolved issues pertaining to the phase diagram of long-fragment DNA: (i) the nature and the ionic strength dependence of the cholesteric \rightarrow LH phase transition and (ii) the connection between this DNA ordering transition in monovalent salts and the DNA condensation transition in polyvalent salts²⁰. By using a new method of finely temperature-tuning the osmotic pressure, we thus find that the cholesteric \rightarrow LH transition in monovalent salts is first order, just like the cholesteric \rightarrow columnar hexagonal transition in short-fragment (≈ 50 nm long) DNA¹⁵, with a small but finite volume change. We also find a *continuity of states*, as opposed to the qualitatively different behavior usually invoked when comparing monovalent and polyvalent salt DNA solutions²⁰, between this ordering transition in monovalent salts and the condensation transition induced by osmotic pressure at subcritical $\text{Co}(\text{NH}_3)_6^{3+}$ (i.e., CoHex) concentration. The elucidation of these features of the DNA phase diagram in various solution conditions is particularly important for the description of DNA packing in bacteriophage capsids^{4–8}, occurring within the same range of DNA densities and osmotic pressures, as well as for understanding the long-range interactions that drive the DNA condensation in polyvalent salts. They have both been the subject of focused theoretical efforts^{21–23}.

Ever since its discovery^{1,24}, the nature of the cholesteric \rightarrow LH transition has remained unresolved and was presumed to be either continuous (second order) or weak first-order with a small volume discontinuity. The implied *caveat* has always been that the available accuracy of osmotic pressure resolution does not allow for a definitive resolution of the order of the transition and that the absence of detectable density discontinuity in the equation of state should not be interpreted as a definitive evidence that the transition is second order. A distinct possibility would thus exist that there is an extremely narrow phase-coexistence window that can not be resolved by the osmotic stress method². However, this phase-coexistence window, on the order of $\sim 1\text{--}2\text{\AA}$ interaxial spacing wide, has now been detected in monovalent salt DNA solutions through high resolution control of the osmotic pressure, based on its known temperature variation²⁵. While not completely unexpected, the existence of this phase-coexistence window in monovalent salt solutions is nevertheless surprising. In fact, phase coexistence at finite osmotic pressures has been heretofore observed only in the case of DNA solutions with polyvalent counterions, e.g., with CoHex, or other condensing agents, when the polyvalent counterion concentration is below a critical value that would induce an immediate precipitation of DNA. In fact, at these subcritical polyvalent salt concentrations DNA condensation does not occur spontaneously but has to be induced by an additional solution osmotic pressure²⁶ that then pushes DNA through a clearly detectable first-order expanded \rightarrow

condensed transition. If the concentration of the polyvalent salt is then increased above a critical value that depends on other solution parameters, DNA condenses spontaneously without any need for an additional osmotic pressure push from the solution. The ensuing DNA condensation transition then becomes second order.

We now connect the existence of the finite density jump for subcritical polyvalent salt solutions with a similar first-order cholesteric \rightarrow LH transition in the case of monovalent (NaCl) salts. This effectively unifies the phase diagrams of DNA for mono- and polyvalent salts and allows us to describe quantitatively the whole regime of DNA equation of state, i.e., the osmotic pressures vs. density dependence, including the volume discontinuity at the cholesteric \rightarrow LH for monovalent salts or expanded \rightarrow condensed DNA transitions for polyvalent salts, with a simple empirical equation of state. It identifies a universal attractive interaction between DNA molecules, even in a monovalent (NaCl) salt, that probably stems from a structural adaptation of DNA helices to the strong interaxial hydration and/or electrostatic interactions at high densities. A picture showing more intimate connection between the nature of the positional, orientational, and bond orientational order^{17,18,27} and the ensuing interaxial interactions between DNA double helices is thus clearly emerging. This change in perspective should be relevant also for understanding the high-density DNA packing in viruses^{4–8,28–30}, where DNA is under high osmotic pressure/high density conditions identical to those studied in our experiments, and on ejection driven by these osmotic stored forces undergoes a series of phase transitions^{7,8} directly related to those addressed in this work. Indeed, the osmotic pressures (≈ 60 atm)^{28,29} and the corresponding DNA interaxial spacings ($\approx 26\text{--}27\text{\AA}$)³¹ are right in the regime studied in this manuscript.

The details of the organization of DNA and genome regulation processes in eukaryotic cells are beyond the scope of this study. Briefly, in eukaryotic cells, DNA is packaged in repeating units, a length of DNA (≈ 50 nm) wound around nucleosomal core particles which consist of positively charged histone proteins³². In this *diffuse* packaging, the DNA molecule and its genome is organized in a way that specific genes are still available for transcription. However, in the compaction of DNA in eukaryotic sperm cells, the histones are replaced with much simpler arginine-rich protamines that pack DNA into a highly condensed hexagonal lattice³⁴, identical to DNA-protamine condensation *in vitro*^{14,33}. The repeating unit of the hexagonal lattice consists of a length of DNA chain and an associated protamine polypeptide chain, as observed in x-ray diffraction of sperm chromatin³⁴, with the polypeptide chain locked in the major groove of the DNA double helix so that the DNA charge is almost completely neutralized^{11,34–36}. The volume occupied by DNA in the sperm cell is small compared with the volume of chromatin in somatic cells. The highly condensed, inactive state of the DNA in sperm nuclei confers additional protection against damage from the effects of mutagens and genotoxic factors^{37–39}.

The study of highly concentrated DNA solutions is thus not only relevant from the fundamental biophysics point of view, but it also sheds light on the molecular mechanisms of DNA packing in bacteriophages and eukaryotic sperm cells. It also constrains possible mechanisms of gene delivery⁴⁰ and illuminates fundamental physical principles that extend to other areas of condensed matter physics^{17,18}.

Results

Our first significant observation is the abrupt change in the DNA density and order at the cholesteric \rightarrow LH transition in NaCl solutions. The abrupt transition, from less-ordered cholesteric phase into the more-ordered LH phase, is evident in the x-ray diffraction behavior of unoriented²⁶ and oriented⁴¹ long-fragment DNA samples. Higher-order peaks in the diffraction intensity profiles confirm hexagonal packing in the LH phase; hexagonal packing is assumed in the cholesteric phase. With our new experimental methodology of finely tuning the osmotic pressure (Π) of PEG solutions via temperature



(T) variations²⁵, the transitions are measured with high accuracy (see Fig. 1). From DNA samples in NaCl solutions at different [PEG] and T (but approximately the same Π), the same interaxial distance (d_{int}) and full width at half-maximum (FWHM) are obtained. The impact of T (i.e., for $15^\circ\text{C} \leq T \leq 45^\circ\text{C}$) on d_{int} and FWHM is thus only through its effect on Π ; changing T in the cases considered does not translate into a direct effect on the interactions between the DNA chains as is the case for, e.g., Mn^{2+} condensation⁴². This is evident in the data shown for $[\text{NaCl}] = 0.1 \text{ M}$ (see Fig. 1) and a large number of similar measurements under $0.05 \text{ M} \leq [\text{NaCl}] \leq 0.4 \text{ M}$. We undertake further measurements of the cholesteric \rightarrow LH transitions based on this fact (see Fig. 2).

In the cholesteric phase, there is a broad first-order x-ray diffraction peak (see Fig. 1). Upon increasing Π , at the cholesteric \rightarrow LH transition, the diffraction intensity profile changes abruptly, and a sharp peak (with FWHM ≈ 5 times bigger than the instrumental resolution) is superimposed on the broad cholesteric peak. In addition, oriented DNA samples, with the helical axis parallel to the x-ray beam, give sixfold symmetric first-order diffraction peaks in the LH phase, indicating *macroscopic* bond orientational order¹ perpendicular to the local axis of the molecules. Disorder in the packing increases with increasing DNA density in the LH phase (see Fig. 1), which points to the possibility of frustrated ordering at high densities²⁷. After progressive disordering at high densities in LH phase, DNA eventually crystallizes through a LH \rightarrow orthorhombic transition (discussed below) into an orthorhombic crystal. Conversely, in the cholesteric phase, we observed further broadening of the diffraction peak with decreasing DNA density. It is also worth emphasizing that in the cholesteric phase the diffraction peak width is sensitive to $[\text{NaCl}]$, and increases with increasing $[\text{NaCl}]$ at fixed DNA density (see Fig. 2).

We measured the osmotic pressure of DNA arrays via the osmotic stress method^{19,43,44}. The osmotic pressure data Π vs. d_{int} , for different $[\text{NaCl}]$ are shown in Fig. 3. In order to parameterize in a simple way the experimentally determined dependence of the osmotic pressure on d_{int} and ionic strength, we invoke a cylindrical cell model formulation of the linearized Poisson-Boltzmann theory⁴⁵. This does not imply that this approximate theory can describe all the details of the DNA-DNA interaction appropriately. Nevertheless it serves the purpose of parsimoniously parameterizing a vast amount of data

by intuitive effective parameters. In this simplified model, a molecule of radius a ($\approx 10\text{\AA}$ for B-DNA) is considered to be surrounded by a cylindrical cell of radius $R = d_{int}/2$, yielding the electrostatic part of the osmotic pressure as

$$\Pi_e(R) = A_e [K_0(R/\lambda_D)/K_1(a/\lambda_D)]^2 \quad (1)$$

to the leading order. Here $K_0(x)$ and $K_1(x)$ are the cylindrical Bessel functions of the second kind. λ_D is the Debye length and $A_e = \sigma^2/\epsilon\epsilon_0$, where σ is the effective surface charge density of DNA, and $\epsilon\epsilon_0$ is the dielectric permittivity of the medium (ϵ_0 is vacuum permittivity and $\epsilon \approx 80$ for water). The effect of T on ϵ , over the range of temperatures used in the measurements, is small and can be ignored. For fully charged B-DNA, $\sigma = e_0/(2\pi ab)$, where e_0 is the elementary charge and $b \approx 1.7\text{\AA}$ is the linear density of phosphates on the DNA. In LH phase, where conformational fluctuation effects are negligible, the net repulsion is equal to the bare interaction osmotic pressure, i.e., $\Pi_0(R) = \Pi_h(R) + \Pi_e(R)$. The hydration repulsion⁴⁶, $\Pi_h(R)$, being the universal short-range component of the interactions, can be described phenomenologically by the same formalism as the electrostatic repulsion, with

$$\Pi_h(R) = A_h [K_0(R/\lambda_h)/K_1(a/\lambda_h)]^2. \quad (2)$$

LH phase data sets for each $[\text{NaCl}]$ are fitted simultaneously to Π_0 . The common hydration repulsion parameters (A_h and λ_h) are enforced to be the same for all $[\text{NaCl}]$. The dependencies of A_e and A_h on d_{int} were neglected, an approximation we discuss later. We simultaneously fitted different combinations of two out of four data sets. A_h and λ_h were linked for all $[\text{NaCl}]$, while A_e was allowed to be different for different $[\text{NaCl}]$. In addition, for each $[\text{NaCl}]$, the Debye decay length was allowed to vary within $\pm 3\%$ from its calculated value using $\lambda_D = 3.08\text{\AA} / \sqrt{I(M)}$, where $I(M)$ is the molar ionic concentration. We found $\lambda_h \approx 2.2\text{\AA}$ with an error $\approx 10\%$ and then performed a global fitting with four data sets. In this step, λ_h was fixed at 2.2\AA , while A_h and A_e were free parameters. A_h was linked for all $[\text{NaCl}]$ and A_e was allowed to be different for different $[\text{NaCl}]$. In this way $A_h = 1019 \text{ atm}$ and $A_e \approx 155 \text{ atm}$, about the same for all $[\text{NaCl}]$, with an uncertainty $\approx 10\%$. The results of the simultaneous fits of the LH phase data to Π_0 are shown in Fig. 3 (see also *SI Appendix* for details). The treatment of the cholesteric and the LH

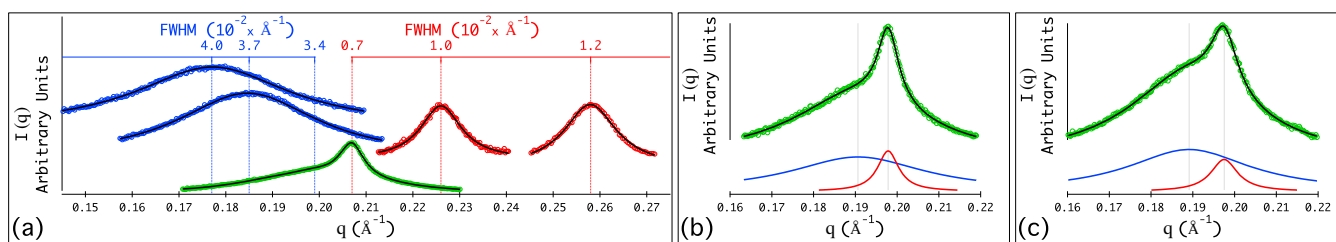


Figure 1 | First-order peaks in the 1D x-ray diffraction intensity profiles of the DNA samples, when $[\text{NaCl}] = 0.1 \text{ M}$, after a linear background is subtracted. The 1D intensity profiles (i.e., $I(q)$ vs. q) are obtained by radial integration of the intensity distributions in the 2D raw x-ray images of the samples. Intensity distributions are fitted (black lines) to either one Lorentzian in the cholesteric (blue) and LH (red) phases or the sum of two Lorentzians in the coexistence region (green). The procedure used for processing x-ray diffraction data and peak fits is described in detail elsewhere²⁵. $I(q)$ is the scattering intensity, with q being the scattering wave vector, i.e., $q = (4\pi/\lambda)\sin(\theta/2)$, where θ is the scattering angle and λ is the x-ray wavelength. The interaxial distances between the neighboring DNA chains (d_{int}) are determined from the peak positions (q_{max}) as $d_{int} = (2/\sqrt{3})d_{Bragg}$, where $d_{Bragg} = 2\pi/q_{max}$. (a): First-order diffraction peaks when $[\text{PEG}] = 20 \text{ wt\%}$, 22 wt\% , 25 wt\% , 30 wt\% , and 40 wt\% with temperature fixed at $T = 40^\circ\text{C}$ (with corresponding pressures $\Pi = 5.3 \text{ atm}$, 6.7 atm , 9.5 atm , 15.6 atm , and 38.3 atm)^{19,43} from left to right, respectively. At low pressures ($\Pi = 5.3 \text{ atm}$ and 6.7 atm), the DNA precipitate is in the cholesteric phase, where the full width at half-maximum (FWHM) of the first-order peak is $\approx 0.035\text{\AA}^{-1}$ (increases with increasing d_{int}). Instrumental resolution and experimental error in the determination of FWHM of the first-order diffraction peaks are $\approx 0.001\text{\AA}^{-1}$ FWHM and vary slightly with q . At high pressures ($\Pi = 15.6 \text{ atm}$ and 38.3 atm), DNA bundles are in the LH phase, which is characterized by a narrow first-order peak, i.e., $\text{FWHM} \approx 0.007\text{\AA}^{-1}$ (increases with decreasing d_{int}). When $\Pi = 9.5 \text{ atm}$, the narrow LH peak is superimposed with the broad cholesteric peak in the diffraction profile. The two distinct types of peaks coexist over a small range of Π , i.e., coexistence region. (b): Phase coexistence observed when $[\text{PEG}] = 22 \text{ wt\%}$ and $T = 30^\circ\text{C}$ (with corresponding pressure $\Pi = 7.7 \text{ atm}$). (c): Phase coexistence observed when $[\text{PEG}] = 20 \text{ wt\%}$ and $T = 15^\circ\text{C}$ (with corresponding pressure $\Pi = 7.4 \text{ atm}$).

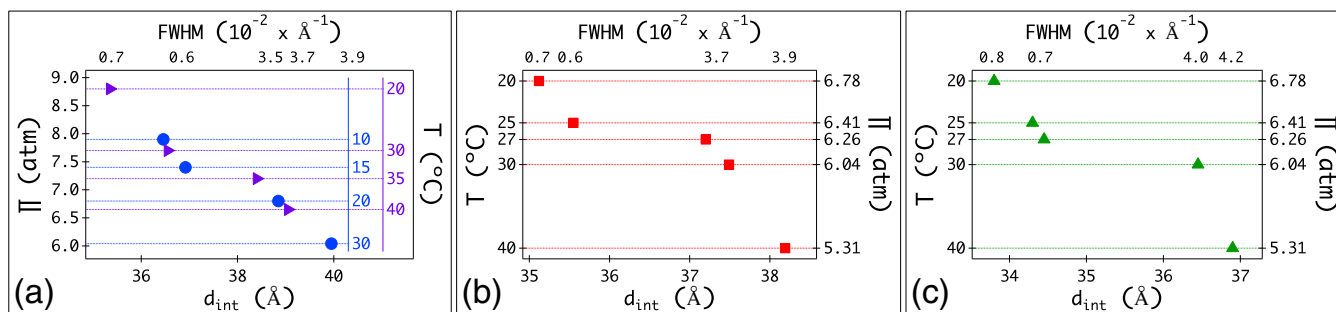


Figure 2 | Examples of the use of temperature variations for fine tuning the osmotic pressure to induce and measure the cholesteric \rightarrow LH transitions. (a), (b), and (c): $[\text{NaCl}] = 0.1 \text{ M}, 0.2 \text{ M},$ and 0.3 M , respectively. In (b) and (c), the left and right axes show temperature variations and the corresponding osmotic pressures Π , respectively, when $[\text{PEG}] = 20 \text{ wt}\%$. It is clearly observed in the $[\text{NaCl}] = 0.1 \text{ M}$ data shown in (b) and (c) in Fig. 1 and a large number of similar measurements at various $[\text{NaCl}]$ (i.e., for $0.05 \text{ M} \leq [\text{NaCl}] \leq 0.4 \text{ M}$) that the only impact of T (i.e., for $15^\circ\text{C} \leq T \leq 45^\circ\text{C}$) on the DNA-DNA interactions is through its effect on Π . Temperature does not have a *detectable* effect on the DNA-DNA interactions in the absence of CoHex over the range of osmotic pressures considered in this study. Under certain concentrations of CoHex, the effect of temperature on the DNA-DNA interactions is also negligible and we can use the same methodology for the fine-measuring of the cholesteric \rightarrow LH transitions (see caption to Fig. 7). DNA samples are equilibrated at each temperature at least one hour before the measurements. Temperature is controlled before and during the measurements using a Peltier device. The biggest interaxial spacings in LH phase ($d_{\text{int,H}}^*$) are determined from x-ray diffraction profiles at the lowest pressures in the coexistence region. Cholesteric phase data points given here are from the diffraction profiles characterized by only the broad peak (without the narrow LH peak), i.e., cholesteric phase data are not shown in the coexistence region. In (a), temperature variations (right axes) and the corresponding pressures (left axis) are shown for two different $[\text{PEG}]$, i.e., $[\text{PEG}] = 20 \text{ wt}\%$ (blue solid circles) and $[\text{PEG}] = 22 \text{ wt}\%$ (purple right-facing triangles). The two right axes in (a) showing the temperature variations are for $[\text{PEG}] = 20 \text{ wt}\%$ and $[\text{PEG}] = 20 \text{ wt}\%$ from left to right, respectively. As explained in the text (see also the caption to Fig. 1), the variations of d_{int} and FWHM with pressure are independent of temperature for all $[\text{NaCl}]$. Note that (a) is adapted from ref. 25.

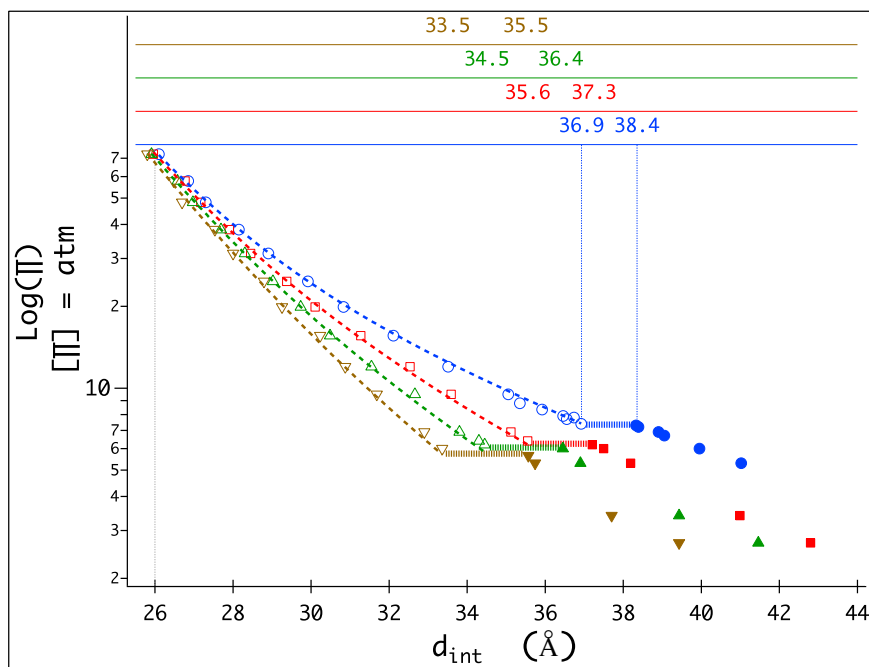


Figure 3 | Osmotic pressure data for different $[\text{NaCl}]$, shown for $d_{\text{int}} \gtrsim 26\text{\AA}^{-1}$. Cholesteric phase data are shown with filled symbols while unfilled symbols represent LH phase data. At low pressures, DNA bundles are in the cholesteric phase. Cholesteric \rightarrow LH transitions take place at transition pressures $\Pi_{tr} \approx 7.4, 6.3, 6.0, 5.8 \text{ atm}$ for $[\text{NaCl}] = 0.1$ (blue circles), 0.2 (red squares), 0.3 (green triangles), 0.4 M (brown inverted triangles), respectively with abrupt changes in d_{int} (from $d_{\text{int,C}}^*$ to $d_{\text{int,H}}^*$) at the transition. Π_{tr} , $d_{\text{int,C}}^*$ and $d_{\text{int,H}}^*$ do not vary significantly for $[\text{NaCl}] \geq 0.4 \text{ M}$. The interaxial separations $d_{\text{int,C}}^*$ and $d_{\text{int,H}}^*$ are given in the top axes for $[\text{NaCl}] = 0.1, 0.2, 0.3, 0.4 \text{ M}$ from bottom to top, respectively. Horizontal lines show the transitions. The overall error in the determination of the interaxial separations in the LH phase with x-ray diffraction is about 0.1\AA . The overall error in the cholesteric phase is bigger (as big as $\approx 0.2\text{\AA}$) due to the positional disorder and broadening of diffraction peaks. Upon increasing osmotic pressure in the LH phase, d_{int} decreases monotonically, and osmotic pressure curves for all $[\text{NaCl}]$ converge. Here data are shown up to the pressure ($\Pi \approx 72 \text{ atm}$) where the differences between the measured d_{int} for the given ionic conditions are $\approx 0.1\text{\AA}$, i.e., close to the uncertainty in the determination of d_{int} . Therefore, in the fits of LH phase data to Π_0 , data from $d_{\text{int}} = d_{\text{int,H}}^*$ to $d_{\text{int}} \approx 26\text{\AA}$ are used. The dashed lines represent the fits for $[\text{NaCl}] = 0.1, 0.2, 0.3, 0.4 \text{ M}$ from top to bottom, respectively.



phase data separately was missing in the available fits in the literature. In addition, the forms for the repulsions and the functions used in those fits are not identical to the forms used in this study. Nevertheless, it was already noted in the literature⁴⁷ that the osmotic pressure data (i.e., Π vs. d_{int}) at small interaxial separations vary exponentially with the decay length reported as 2 to 3 Å. We stress again that the above forms of the electrostatic and the hydration part of the total interaction osmotic pressure should be seen as parsimonious empirical fits rather than attempts at a comprehensive theoretical description of the complicated DNA-DNA interactions that have been reviewed extensively in the literature^{21,22}.

The cholesteric phase of long DNA fragments, being less ordered, gives a broad x-ray diffraction peak with DNA chains fluctuating in their cylindrical cells, leading to positional disorder of the Bragg planes. The fluctuational free energy of DNA molecules is modulated by bare interactions with their neighbors and depends on their bending stiffness. It can be calculated from Frank's elastic free energy for polymer nematics⁴⁸ by integrating out the Gaussian fluctuations around a straight configuration². The fluctuational free energy per DNA chain (F_{fl}), at densities where fluctuations are prominent, is then obtained as

$$F_{fl} \approx k_B T (q_{max})^{5/2} \left[\frac{V_{DNA}}{5 \times 2^{3/2} \times \pi} \left(\frac{B_b}{K} \right)^{1/4} \right] \quad (3)$$

where the wavelength cutoff (i.e., q_{max}) takes into account the molecular size. B_b is the bare bulk compressibility modulus of the DNA cholesteric phase (relative change in the bare interaction pressure with changing cell area), i.e.,

$$B_b = -(\pi R^2) \frac{\partial \Pi_0}{\partial (\pi R^2)}. \quad (4)$$

K is the bending elastic constant defined as $K = \rho K_c$, where ρ is the 2D number density of DNA chains perpendicular to their helical axes and $K_c = (k_B T) L_p$ is the bending rigidity of a single DNA chain. We can ignore the effect of [NaCl] on the persistence length, L_p (≈ 500 Å for B-DNA), as it is less than 5% for $0.1 \text{ M} \leq [\text{NaCl}] \leq 0.4 \text{ M}$ ^{49,50}. V_{DNA} is the volume per DNA chain in the cylindrical cell model, i.e., $V_{DNA} = L(\pi R^2)$, where L is the length of DNA chains. We replace q_{max} with a scaling prefactor (c) times the Brillouin zone (per DNA chain) radius, i.e., $q_{max} \rightarrow c \times (\pi/d_{int})$, which is equivalent to replacing d_{int} with an effective separation, $d_{eff} = d_{int}/c$. Using the thermodynamic relation $\Pi = -\partial F/\partial V$, the osmotic pressure due to fluctuations is

$$\Pi_{fl}(R) = \Pi_{fl}^* \left(-(\pi R^2) \frac{\partial \log B_b}{\partial (\pi R^2)} \right) \quad (5)$$

with

$$\Pi_{fl}^*(R) = \frac{F_{fl}(R)/L}{4\pi R^2} \approx \frac{13.8 \times c^{5/2} \times B_b^{1/4}}{R^2} \text{ atm} \quad (6)$$

when R and B_b are in units of Å and atm, respectively. The total repulsion in the cholesteric phase is described as $\Pi_{cho}(R) = \Pi_0(R) + \Pi_{fl}(R)$. The fits of the cholesteric phase osmotic pressure data to $\Pi_{cho}(R)$ (shown in Fig. 4) yield $c \approx 3$. Calculations, fits, and variations of B_b , F_{fl} , Π_{fl}^* , and Π_{fl} with R for each [NaCl] are explained in detail in *SI Appendix*.

A discontinuous change in d_{int} , i.e., from $d_{int,C}^*$ to $d_{int,H}^*$, at the transition osmotic pressure Π_{tr} , for cholesteric \rightarrow LH transition then results from the balance between the osmotic pressure in the cholesteric phase, Π_{cho} , containing a strong fluctuation contribution, and the osmotic pressure in the LH phase, composed of the bare repulsive interaction pressure Π_0 plus an effective attractive component ($\tilde{\Pi}_{ea}$) viz. diminished repulsion, analogous to the interaction decomposition in the case of the van der Waals gas transition. The contribution of the conformational fluctuations to the osmotic pressure in the much stiffer LH phase is assumed to be nil. $\tilde{\Pi}_{ea}$ increases with increasing [NaCl]. In addition, there is a common decay length at small interaxial distances, as can be discerned clearly in Fig. 5. We propose that the effective attraction follows the same form as the bare interaction repulsion, i.e., the sum of two terms accounting for the two interactions of different origin, with different characteristic decay lengths,

$$\tilde{\Pi}_{ea}(R) = \tilde{A}_h \left[\frac{K_0 \left(R/\tilde{\lambda}_h \right)}{K_1 \left(a/\tilde{\lambda}_h \right)} \right]^2 + \tilde{A}_e \left[\frac{K_0 \left(R/\tilde{\lambda}_e \right)}{K_1 \left(a/\tilde{\lambda}_e \right)} \right]^2 \quad (7)$$

where $\tilde{\lambda}_h$ and $\tilde{\lambda}_e$ are proportional to λ_h and λ_D in Π_0 , respectively, i.e., $\tilde{\lambda}_h = f_h \lambda_h$ and $\tilde{\lambda}_e = f_e \lambda_D$. The parameters \tilde{A}_h , \tilde{A}_e as well as f_h , f_e were determined from the fits of $\tilde{\Pi}_{ea}$ vs. d_{int} data to $\tilde{\Pi}_{ea}$ by further assuming $f = f_h = f_e$ (see Fig. 5 and *SI Appendix* for details). The effective attractive component in the total osmotic pressure, $\Pi_0 + \tilde{\Pi}_{ea}$, then yields a discontinuous first-order transition by the application of the standard Maxwell equal-area construction. We obtain a common $\tilde{A}_h \approx 14$ atm for all [NaCl], with an uncertainty $\approx 10\%$. The parameter attributed to the electrostatic interactions $\tilde{A}_e \approx 17, 20, 24, 27$ atm for [NaCl] = 0.1, 0.2, 0.3, 0.4 M, respectively. The common short-range component suggests the structural adaptation of the DNA chains to hydration interactions at high densities. Furthermore, the variations of the magnitude and decay length of the effective attraction, as well as the variation of Π_{tr} , with salt (as evidenced on Fig. 5) imply the contribution due to electrostatic effects.

We proceed to thermodynamic analysis of the data. The change in the free energy per DNA chain (per unit length) upon changing the DNA density from cell radius R_1 to R_2 is

$$(W/L)_{R_1 \rightarrow R_2} = \int_{R_1}^{R_2} \Pi(R) d(\pi R^2) \quad (8)$$

At the cholesteric \rightarrow LH transitions, where the radius changes abruptly from $R = R_C^*$ to $R = R_H^*$, the free energy change is

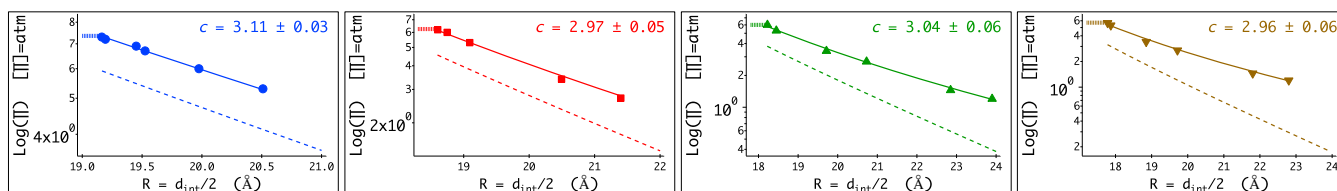


Figure 4 | Cholesteric phase data fits. Colors, symbols, and [NaCl] are the same as in Fig. 3. Dashed lines are the bare interaction pressures, $\Pi_0(d_{int})$, calculated using the parameters extracted from LH phase data fittings (see Fig. 3). Solid lines show the fits of the cholesteric phase data to $\Pi_{cho}(d_{int})$. Each data set for each [NaCl] is fitted individually, and the prefactor c is extracted from the fits as given on top right for each [NaCl]. It is independent of the ionic strength, i.e., $c \approx 3$. Horizontal lines show the transitions from cholesteric phase to LH phase.

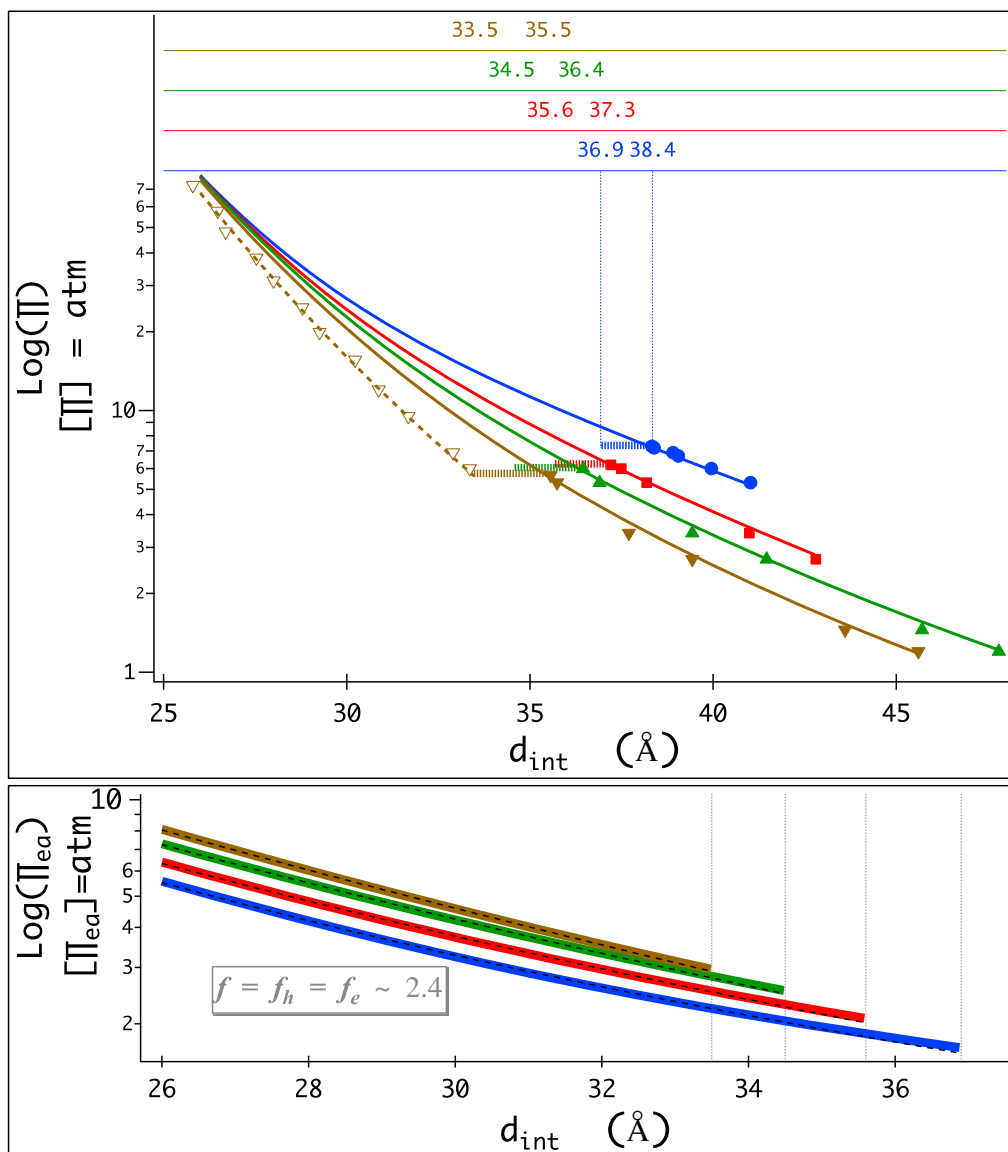


Figure 5 | The application of the standard Maxwell equal-area construction in order to extract the effective attractive component Π_{ea} in the total osmotic pressure. Colors, symbols, and $[\text{NaCl}]$ are the same as in Fig. 3. Top panel: Solid lines show the net repulsion with the fluctuation part, i.e., fits of the cholesteric phase data to $\Pi_{cho}(d_{int})$. They converge at high pressures. In the LH phase, there are no fluctuation effects and the net repulsion is equal to $\Pi_0(d_{int})$. Brown dashed line shows $\Pi_0(d_{int})$ for $[\text{NaCl}] = 0.4$ M in LH phase. Bottom panel: Thick colored lines show $\Pi_{ea}(d_{int})$. Each line ends at $d_{int} = d_{int,H}^*$ due to the transition to the cholesteric phase, where $\Pi_{att} = 0$. From the simultaneous fits of Π_{ea} vs. d_{int} data to $\tilde{\Pi}_{ea}$ (thin black dashed lines), we extract the decay length ratios, $f = f_h = f_e \approx 2.4$ (see SI Appendix for the details).

$$(W/L)_{tr} = \Pi_{tr} [\Delta(\pi R^2)] \quad (9)$$

where $[\Delta(\pi R^2)] = \pi \left[(R_C^*)^2 - (R_H^*)^2 \right]$ is the change in the cell area across the transition. The change in the number of Na^+ ions (per length) with the change in DNA cell radius, $(\Delta N/L)$, can be calculated using Maxwell cross relation, $-(\partial \Pi / \partial \mu) = (\partial N / \partial V)$, which with $V = L(\pi R^2)$ reduces to

$$(\Delta N/L)_{R_1 \rightarrow R_2} = - \frac{\partial}{\partial \mu} (W/L)_{R_1 \rightarrow R_2}, \quad (10)$$

where μ is the chemical potential of the salt, i.e., NaCl . The above relation implies that as the concentration of DNA varies due to the imposed osmotic pressure, the salt is taken up from the bulk reservoir and is redistributed within the DNA subphase, all the while keeping the full electroneutrality of the system. While the detailed nature of

this redistribution cannot be derived without a microscopic model of the ionic atmosphere around the DNA molecule, the change in the number of salt ions in the DNA subphase would indicate that it is indeed taking place. In addition, we will show that most of the changes in the distribution of ions around DNA takes place within the cholesteric phase.

In what follows we assume that the chemical potential of the salt has the ideal form, i.e., $\mu = k_B T \log[\text{NaCl}]$. While in the concentration range 0.1 M to 0.4 M the activity coefficient of NaCl is clearly not equal to 1 and its behavior is not ideal, the chemical potential of the salt appears only in derivative and thus only its changes are important. The change in the activity coefficient of NaCl over the range of concentrations used in our experiments is about 10%⁵¹ and the final effect of the assumption of ideality is less than other sources of error in the determination and analysis of the data.



We consider three regions separately in the analysis: (1) cholesteric phase (from $R \rightarrow \infty$ to $R = R_C^*$); (2) cholesteric \rightarrow LH transition region (from $R = R_C^*$ to $R = R_H^*$); (3) LH phase (from $R = R_H^*$ to $R = R_0$). We calculate the change in the number of Na^+ ions per DNA base pair, $(\Delta N/bp)_C$, $(\Delta N/bp)_{tr}$, and $(\Delta N/bp)_H$, in regions (1), (2), and (3), respectively. Here R_0 is the smallest cell radius in LH phase, with clearly discernible hexagonal symmetry in the x-ray diffraction pattern. For larger DNA densities the hexagonal symmetry is lost and the LH \rightarrow orthorhombic transition ensues. Using the quadratic and line fits in Fig. 6 (see also *SI Appendix* for the details of the calculations), we find $(\Delta N/bp)_H = 0.59$, $(\Delta N/bp)_{tr} = 0.01$ and $(\Delta N/bp)_C = 1.76 - 0.65 \log[\text{NaCl}]$ with $[\text{NaCl}]$ in mM.

These results suggest that the change in the number of Na^+ ions in the DNA subphase is independent of $[\text{NaCl}]$ at the transition and in the LH phase (discussed later). However, $(\Delta N/bp)_C$ varies with $[\text{NaCl}]$ and upon changing the DNA density from infinite dilution up to the cholesteric \rightarrow LH transition, about 23%, 13%, 7%, and 3% of the bare DNA charge is neutralized at $[\text{NaCl}] = 0.1, 0.2, 0.3, 0.4$ M, respectively, if we assume that of the salt ions taken up by the DNA subphase, Na^+ ends up being located in close proximity to the DNA charges. There is thus a detectable difference in the number of Na^+ ions near DNA phosphates under different $[\text{NaCl}]$ at the infinite dilution limit and at a finite concentration in the cholesteric phase.

For short-fragment (≈ 50 nm long) DNA, in NaCl solutions, the hexagonal \rightarrow orthorhombic transition occurs near DNA density corresponding to $d_{int} = 23.7 \text{ \AA}$ ¹⁵. Lindsay *et al.*⁵² showed that long Na-DNA fibers also go through a similar transition at around 90% relative humidity that, in addition, coincides with a B to A conformational transition of DNA with a helical pitch length change from $\approx 34 \text{ \AA}$ for B-form to $\approx 29 \text{ \AA}$ for A-form. In the orthorhombic phase the DNA density does not change anymore upon further drying⁵². Our osmotic stress experiments, in which the water content of DNA is accurately controlled and the corresponding osmotic pressures are known, indicate that on increase of the osmotic pressure in LH phase the first-order x-ray diffraction peak first broadens, followed by the LH \rightarrow orthorhombic transition at $\Pi \approx 170$ atm, characterized by the complete disappearance of the hexagonal symmetry of the scattering intensity (see Fig. 7).

The order of the cholesteric \rightarrow LH transition in NaCl solutions, together with its equation of state and the pertinent Maxwell

equal-area construction, are relevant also for DNA condensation transition induced by osmotic pressure at subcritical CoHex concentrations (see Fig. 7). Obviously the subcritical condensation transition (i.e., abrupt change in the volume per base pair (v_{bp}) and the ensuing collapse of DNA into a highly ordered structure, induced by osmotic pressure, in the presence of low concentrations of polyvalent salts) bears a striking similarity to the cholesteric \rightarrow LH transition in NaCl solutions even in terms of the identical diffraction fingerprint. The cholesteric \rightarrow LH transition thus exists also at subcritical [CoHex] in osmotic pressure-induced condensation of long DNA, i.e., for any $[\text{CoHex}] \leq [\text{CoHex}]^*$, where $[\text{CoHex}]^*$ is the minimum critical [CoHex] necessary for condensation at zero osmotic pressure. We find that $[\text{CoHex}]^* = 28$ mM in $[\text{NaCl}] = 0.3$ M solutions. The osmotic pressure-induced transitions for $[\text{CoHex}] = 0$, $[\text{CoHex}] = 3$ mM, and $[\text{CoHex}] = 12$ mM at $[\text{NaCl}] = 0.3$ M are shown in Fig. 7. With increasing [CoHex], Δv_{bp} increases and Π_{tr} decreases. The effective attraction leading to the first-order condensation transition, that can be deduced in the same way as in the monovalent salt case, increases with the addition of CoHex in the solution.

These results point to a continuity of thermodynamic states between the cholesteric \rightarrow LH transition in monovalent salts and DNA polyvalent salt-induced condensation, frequently viewed as completely distinct phenomena. In fact, addition of CoHex (at subcritical concentrations) simply increases Δv_{bp} at the cholesteric \rightarrow LH transition already present in NaCl solutions. As the polyvalent salt concentration increases, the cholesteric branch density first moves to higher values, following the LH branch, but then eventually starts moving toward lower densities. At the critical concentration of the polyvalent salt, it moves out to infinity, i.e., the DNA condenses at zero external osmotic pressure. This last part of the polyvalent salt dependence is experimentally difficult to quantify⁵³, but the existence of the condensation at zero imposed osmotic pressure indicates that indeed the cholesteric branch must recede to infinite dilution at the critical concentration.

Discussion

With increasing osmotic pressure, delicately controlled with small temperature variations²⁵, DNA undergoes a transition from a less ordered fluctuating (cholesteric) state to a more ordered LH state

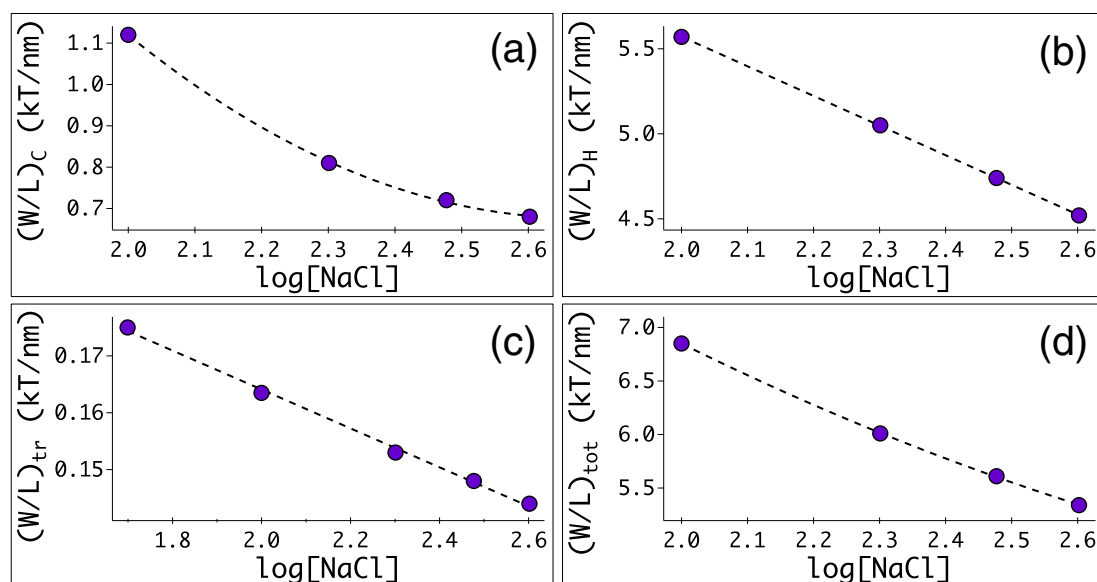


Figure 6 | Calculated free energy per length, (W/L) , vs. $\log[\text{NaCl}]$ in different regions of the phase diagram. $[\text{NaCl}]$ is in mM concentration units. (a): Cholesteric phase. (b): LH phase. (c): Cholesteric \rightarrow LH transition. (d): From $R \rightarrow \infty$ to $R = R_0$. Black dashed curves are quadratic (a and d) and line (b and c) fits.

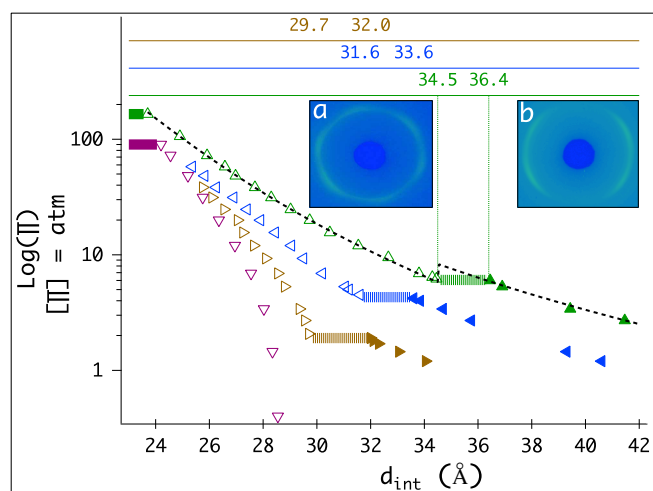


Figure 7 | Osmotic pressure-induced transitions for different [CoHex] at [NaCl] = 0.3 M. Horizontal dashed lines show the cholesteric \rightarrow LH transitions. Horizontal solid lines show the LH \rightarrow orthorhombic transitions. For [CoHex] = 3 mM (blue left-facing triangles) and [CoHex] = 12 mM (brown right-facing triangles), data are shown up to the pressure where d_{int} is approximately 0.1 Å bigger than the interaxial distance measured when [CoHex] = [CoHex]^{*} = 28 mM (purple inverted triangles); above that they superimpose with [CoHex]^{*} data. Black dashed curve (with jump at the transition) is the fit of [CoHex] = 0 (green triangles) data to the total osmotic pressure. At less than [CoHex]^{*}, the dependence of osmotic pressure on d_{int} is slightly sensitive to temperature at low pressures ($\Pi \lesssim 2.5$ atm) and [CoHex] = [CoHex]^{*} data is shown only for $T = 20^\circ\text{C}$. No detectable temperature dependence for other [CoHex] (see *SI Appendix* and ref. 25 for details) and the transitions can be measured with high accuracy using temperature variations. Insets: Typical x-ray images of oriented DNA bundles in LH phase with DNA helical axis parallel and perpendicular to the x-ray beam in (a) and (b), respectively. The sixfold symmetry in (a) shows the long-range bond orientational order in the LH phase. This symmetry does not exist in the x-ray images of DNA samples in the cholesteric phase. The twofold symmetry in (b) shows the parallel alignment of DNA chains. In the oriented sample preparations⁴¹, we align the bundles of DNA chains in the same direction in order to make *macroscopically* oriented samples so that 2D ordering of DNA chains can be seen in the x-ray images. The angular widths of the arcs are due to the mosaic spread in our samples.

with negligible conformational fluctuations. Changes in DNA density and packing at the cholesteric \rightarrow LH transition are discontinuous, as observed in the x-ray scattering of long DNA fragments. We measured this transition with high accuracy and investigated its sensitivity to solution conditions. The sixfold symmetric azimuthal intensity profile of the first-order diffraction peak in the x-ray images of oriented DNA suggests that long-fragment DNA packs in a straight parallel untwisted arrangement in the LH phase, with long-range bond orientational order perpendicular to the axis of the molecules^{1,24}. At the transition from the more ordered LH phase to the cholesteric phase, the sixfold azimuthal symmetry in the diffraction peak disappears; the vanishing of long-range bond orientational order and the abrupt change in DNA density occur simultaneously.

The osmotic pressure and inverse ionic strength dependence of the cholesteric \rightarrow LH transition is similar to the pressure and temperature dependence of the gas-liquid transition, i.e., cholesteric \rightarrow LH transition is shifted to higher osmotic pressures upon decreasing ionic strength of the solution. Furthermore, Δv_{bp} at the cholesteric \rightarrow LH transition decreases, and DNA osmotic pressure curves become progressively more flat around the transition region with

decreasing ionic strength. When $[\text{NaCl}] = 50 \text{ mM}$ (the smallest [NaCl] for which we measured the cholesteric \rightarrow LH transition), and for $\Pi \lesssim 9$ atm the first-order x-ray diffraction peak is lost because of strong electrostatic repulsion. For this reason, [NaCl] = 50 mM data (available only for $\Pi \gtrsim 9$ atm and shown in *SI Appendix*) were not used in the simultaneous $\Pi_{\text{cho}}(d_{\text{int}})$ fits. For [NaCl] = 50 mM, the transition in fact occurs at $\Pi_{\text{tr}} = 9.7$ atm, and the abrupt change in the interaxial distance (Δd_{int}) is 1.2 Å ($d_{\text{int,C}}^* = 39.1$ Å and $d_{\text{int,H}}^* = 37.9$ Å). With increasing [NaCl], Π_{tr} decreases and Δd_{int} increases. For [NaCl] = 0.4 M, $\Pi_{\text{tr}} = 5.8$ atm and $\Delta d_{\text{int}} = 2$ Å, they do not vary any more upon further increase in [NaCl].

The estimated value for the effective charge $A_e = \sigma^2 / \epsilon \epsilon_0$ (see Eq. 1) from the simultaneous fits of LH phase data is ≈ 155 atm (approximately the same for all [NaCl], with an uncertainty $\approx 10\%$). For fully charged DNA chains, A_e would be approximately twice as large as what we extracted from the fits. If the parameter A_e is a measure of the net charge, then about half the bare DNA charge is neutralized in the LH phase. Conversely, if the net charge decreases with increasing DNA density, then one would also expect A_e to decrease with increasing DNA density. The change in the number of Na^+ ions from cholesteric \rightarrow LH transition up to the LH \rightarrow orthorhombic transition, is $(\Delta N/bp)_H = 0.59$ and is independent of [NaCl].

The fact that $(\Delta N/bp)_H$ is independent of [NaCl] is instructive. Combined with the observation that the osmotic pressure curves converge at high pressures, it suggests that the number of salt ions per base pair is already the same for all [NaCl] at the cholesteric \rightarrow LH transition and that the transition occurs when the net charge drops to a certain value. $\tilde{\Pi}_{\text{ea}}$ is zero in the cholesteric phase, i.e., when the net DNA charge is above a certain limit. Lee *et al.*⁵⁴ predict similar transitions of DNA in NaCl solutions and underline the role of structural adaptation of DNA helices to the interactions which is a function of ionic conditions and d_{int} . Their theory predicts a ratio of ≈ 2 between the decay lengths for attractive and repulsive interactions²¹. In our experiments, the measured effective attraction Π_{ea} is approximately an order of magnitude smaller than the net repulsion in LH phase Π_0 . The magnitude of Π_{ea} is also sensitive to the ionic strength and decreases with decreasing [NaCl] (see Fig. 5). The ratio of the decay length of Π_{ea} to the decay length of Π_0 is extracted by fitting the osmotic pressure data. The obtained factor $f = f_h = fe \approx 2.4$ is reasonable, although our analysis was based on several simplifying assumptions.

The emerging connection between the cholesteric \rightarrow LH transition in univalent NaCl solution and the DNA condensation transition in the presence of polyvalent salts²⁶, such as CoHex, at subcritical concentrations indicates a major change in DNA behavior in various solution conditions. We observe that osmotic pressure-induced DNA condensation at subcritical [CoHex] occurs in the same way as the cholesteric \rightarrow LH transition in NaCl solutions. Our experiments now reveal that the osmotic pressure-induced condensation of long DNA indeed occurs at all polyvalent salt concentrations, for example at any [CoHex] \leq [CoHex]^{*}, where [CoHex]^{*} is the minimum [CoHex] necessary for condensation at zero osmotic pressure. It depends also on the concentration of monovalent salt so that when [NaCl] = 0.3 M, [CoHex]^{*} = 28 mM. With increasing [CoHex], Δv_{bp} increases slightly, and the transition pressure Π_{tr} decreases. With the addition of CoHex to the bathing solution, the effective attraction therefore increases.

The general similarity between these two transitions therefore points to a continuity of thermodynamic states between the cholesteric \rightarrow LH transition and the osmotic pressure-induced DNA condensation transition at subcritical [CoHex], thus bridging the gap between superficially distinctly different behaviors of DNA in monovalent and polyvalent salt bathing solutions.

Methods

Sample preparation and data collection. Oriented⁴¹ and unoriented^{25,26} DNA samples are prepared using calf thymus or salmon sperm DNA (molecular weight \approx



10^7 Daltons). Oriented fibers are prepared by wet-spinning using the apparatus (designed by A. Rupprecht) in ILL (Grenoble, France). X-ray diffraction measurements are made using our in-house setup²⁵ at UMass Amherst. Diffraction peak fits are done using IGOR Pro multi-peak fitting package. Brief explanations of x-ray diffraction data collection and analysis are given in the caption to Fig. 1. See also ref. 25 and *SI Appendix* for more details on sample preparations and data collection.

Osmotic pressure data. Temperature-dependent osmotic pressure data of PEG (molecular weight of 8000 Daltons) solutions are from ref. 19. Osmotic pressure decreases almost linearly with increasing T at constant $[\text{PEG}]$ for $20^\circ\text{C} \leq T \leq 40^\circ\text{C}$. The osmotic pressure of PEG, as well as the temperature dependence of the osmotic pressure of PEG, are not new. They have been described, analyzed, and used for decades, being also extensively documented in various publications and reproduced by a variety of experimental methods (e.g., vapor pressure osmometer, membrane osmometer). In addition, the effect of salt on PEG activity (measured at room temperature by Wescor vapor pressure osmometer 5600) is insignificant at salt concentrations used in the experiments.

Cholesteric \rightarrow LH transition measurements. The novel methodology used in this study takes advantage of the dependence of PEG (molecular weight of 8000 Daltons) osmotic pressure on temperature in order to achieve a heretofore unattained accuracy in fixing the value of this pressure. This enables also a much-improved accuracy in the determination of the equation of state of DNA (i.e., Π vs. d_{int}), which reveals additional fine features of this equation of state that have been previously missed, enabling a deeper insight into the behavior of DNA at high concentrations. Note that using temperature to vary the osmotic pressure of the PEG solution in equilibrium with a DNA subphase is possible because under certain conditions, DNA-DNA interactions are almost independent of temperature over the range 15°C to 45°C . We therefore take advantage of the fact that temperature has no detectable effect on the DNA-DNA interactions to use it to accurately set the osmotic pressure of the DNA solution. The use of temperature variation methodology to measure the cholesteric \rightarrow LH transitions is described briefly in the captions to Fig. 1 and Fig. 2. See also ref. 25 and *SI Appendix* for more details.

- Podgornik, R. *et al.* Bond orientational order, molecular motion, and free energy of high-density DNA mesophases. *Proc. Natl. Acad. Sci. USA* **93**, 4261–4266 (1996).
- Strey, H. H., Parsegian, V. A. & Podgornik, R. Equation of state for polymer liquid crystals: Theory and experiment. *Phys. Rev. E* **59**, 999–1008 (1999).
- Rey, A. D. Liquid crystal models of biological materials and processes. *Soft Matter* **6**, 3402–3429 (2010).
- Ross, W. H., Bruinsma, R. & Wuite, G. J. L. Physical virology. *Nature Phys.* **6**, 733–743 (2010).
- Knobler, C. M. & Gelbart, W. M. Physical Chemistry of DNA Viruses. *Annu. Rev. Phys. Chem.* **60**, 367–383 (2009).
- Keller, N., delToro, D., Grimes, S., Jardine, P. J. & Smith, D. E. Repulsive DNA-DNA interactions accelerate viral DNA packaging in phage phi29. *Phys. Rev. Lett.* **112**, 248101 (2014).
- Leforestier, A. & Livolant, F. The bacteriophage genome undergoes a succession of intracapsid phase transitions upon DNA ejection. *J. Mol. Biol.* **396**, 384–395 (2010).
- Lemay, S. G., Panja, D. & Molineux, I. J. Role of osmotic and hydrostatic pressures in bacteriophage genome ejection. *Phys. Rev. E* **87**, 022714 (2013).
- De Jonge, C. J. & Barratt, C. L. R. *The sperm cell: production, maturation, fertilization, regeneration* (Cambridge University Press, Cambridge, 2006).
- Balhorn, R. An Overview. *Sperm Chromatin: Biological and Clinical Applications in Male Infertility and Assisted Reproduction* (Springer, New York, 2011).
- Herskovits, T. T. & Brahmans, J. Structural investigations on DNA-protamine complexes. *Biopolymers* **15**, 687–706 (1976).
- Balhorn, R. A model for the structure of chromatin in mammalian sperm. *J. Cell Biol.* **93**, 298–305 (1982).
- Toma, A. C., de Frutos, M., Livolant, F. & Raspaud, E. Phase diagrams of DNA and poly(styrene-sulfonate) condensed by a poly-cationic protein, the salmon protamine. *Soft Matter* **7**, 8847–8855 (2011).
- DeRouchey, J. E., Hoover, B. & Rau, D. C. A comparison of DNA compaction by arginine and lysine peptides: A physical basis for arginine rich protamines. *Biochemistry* **52**, 3000–3009 (2013).
- Durand, D., Doucet, J. & Livolant, F. A study of the structure of highly concentrated phases of DNA by x-ray diffraction. *J. Phys. II France* **2**, 1769–1783 (1992).
- Leforestier, A. & Livolant, F. Supramolecular ordering of DNA in the cholesteric liquid crystalline phase: An ultrastructural study. *Biophys. J.* **65**, 56–72 (1993).
- Chaikin, P. M. & Lubensky, T. C. *Principles of Condensed Matter Physics* (Cambridge University Press, Cambridge, 1995).
- Nelson, D. R. Vortex lattice melts like ice. *Nature* **375**, 356–357 (1995). Bruun, G. M. & Nelson, D. R. Quantum hexatic order in two-dimensional dipolar and charged fluids. *Phys. Rev. B* **89**, 094112 (2014).
- Parsegian, V. A., Rand, R. P., Fuller, N. L. & Rau, D. C. Osmotic stress for the direct measurement of intermolecular forces. *Meth. Enzym.* **127**, 400–416 (1986).
- Bloomfield, V. A. DNA condensation. *Curr. Opin. Struct. Biol.* **6**, 334–341 (1996).
- Kornyshev, A. A., Lee, D. J., Leikin, S. & Wynveen, A. Structure and interactions of biological helices. *Rev. Mod. Phys.* **79**, 943–996 (2007).
- Cherstvy, A. G. Electrostatic interactions in biological DNA-related systems. *Phys. Chem. Chem. Phys.* **13**, 9942–9968 (2011).
- Naji, A., Kanduc, M., Forsman, J. & Podgornik, R. Perspective: Coulomb fluids - weak coupling, strong coupling, in between and beyond. *J. Chem. Phys.* **139**, 150901 (2013).
- Strey, H. H. *et al.* Refusing to twist: Demonstration of a line hexatic phase in DNA liquid crystals. *Phys. Rev. Lett.* **84**, 3105–3108 (2000).
- Yasar, S., Podgornik, R. & Parsegian, V. A. Continuity of states in cholesteric - line hexatic transition in univalent and polyvalent salt DNA solutions. *MRS Proceedings* **1619**, mrsf13-1619-a05-02; DOI:10.1557/opl.2014.358 (2013).
- Rau, D. C. & Parsegian, V. A. Direct measurement of the intermolecular forces between counterion-condensed DNA double helices. Evidence for long-range attractive hydration forces. *Biophys. J.* **61**, 246–259 (1992).
- Lorman, V., Podgornik, R. & Žekš, B. Positional, reorientational, and bond orientational order in DNA mesophases. *Phys. Rev. Lett.* **87**, 218101 (2001).
- Smith, D. E. *et al.* The bacteriophage phi29 portal motor can package DNA against a large internal force. *Nature* **413**, 748–752 (2001).
- Molineux, I. J. Fifty-three years since Hershey and Chase; much ado about pressure but which pressure is it? *Virology* **344**, 221–229 (2006).
- Evilleitch, A., Castelnuovo, M., Knobler, C. M. & Gelbart, W. M. Measuring the force ejecting DNA from phage. *J. Phys. Chem. B* **108**, 6838–6843 (2004).
- Earnshaw, W. C. & Harrison, S. C. DNA arrangement in isometric phage heads. *Nature* **268**, 598–602 (1977).
- McGhee, J. D. & Felsenfeld, G. Nucleosome Structure. *Ann. Rev. Biochem.* **49**, 1115–1156 (1980).
- Motta, S. *et al.* Nanoscale structure of protamine/DNA complexes for gene delivery. *Appl. Phys. Lett.* **102**, 053703 (2013).
- Feughelman, M. *et al.* Molecular structure of deoxyribose nucleic acid and nucleoprotein. *Nature* **175**, 834–838 (1955).
- Hud, N. V., Milanovich, F. P. & Balhorn, R. Evidence of novel secondary structure in DNA-bound protamine is revealed by Raman spectroscopy. *Biochemistry* **33**, 7528–7535 (1994).
- Prieto, M. C., August, H. M. & Balhorn, R. Analysis of DNA-Protamine Interactions by Optical Detection of Magnetic Resonance. *Biochemistry* **36**, 11944–11951 (1997).
- Suzuki, M., Crozatier, C., Yoshikawa, K., Mori, T. & Yoshikawa, Y. Protamine-induced DNA compaction but not aggregation shows effective radioprotection against double-strand breaks. *Chem. Phys. Lett.* **480**, 113–117 (2009).
- Dominguez, K., Arca, C. D. R. & Ward, W. S. The Relationship Between Chromatin Structure and DNA Damage in Mammalian Spermatozoa. *Sperm Chromatin: Biological and Clinical Applications in Male Infertility and Assisted Reproduction* (Springer, New York, 2011).
- Agarwal, A. & Said, T. M. Role of sperm chromatin abnormalities and DNA damage in male infertility. *Hum. Reprod. Update* **9**, 331–345 (2003).
- Podgornik, R., Harries, D., DeRouchey, J., Strey, H. H. & Parsegian, V. A. Interactions in Macromolecular Complexes Used as Nonviral Vectors for Gene Delivery. *Gene Therapy: Therapeutic Mechanisms and Strategies* (Marcel Dekker, New York, 2008).
- Rupprecht, A. Preparation of oriented DNA by wet spinning. *Acta. Chem. Scand.* **20**, 494–504 (1966).
- Rau, D. C. & Parsegian, V. A. Direct measurement of temperature-dependent solvation forces between DNA double helices. *Biophys. J.* **61**, 260–271 (1992).
- Stanley, C. B. & Strey, H. H. Measuring osmotic pressure of poly(ethylene glycol) solutions by sedimentation equilibrium ultracentrifugation. *Macromolecules* **36**, 6888–6893 (2003).
- Beck, R., Deek, J., Jones, J. B. & Safinya, C. R. Gel-expanded to gel-condensed transition in neurofilament networks revealed by direct force measurements. *Nature Mater.* **9**, 40–46 (2010).
- Fuoss, R., Katchalsky, A. & Lifson, S. The potential of an infinite rod-like molecule and the distribution of the counterions. *Proc. Natl. Acad. Sci. USA* **37**, 579–589 (1951).
- Marčelja, S. & Radić, N. Repulsion of interfaces due to boundary water. *Chem. Phys. Lett.* **42**, 129–130 (1976).
- Stanley, C. & Rau, D. C. Evidence for water structuring forces between surfaces. *Curr. Opin. Colloid Interface Sci.* **16**, 551–556 (2011).
- Grason, G. M. Braided bundles and compact coils: The structure and thermodynamics of hexagonally packed chiral filament assemblies. *Phys. Rev. E* **79**, 041919 (2009).
- Baumann, C. G., Smith, S. B., Bloomfield, V. A. & Bustamante, C. Ionic effects on the elasticity of single DNA molecules. *Proc. Natl. Acad. Sci. USA* **94**, 6185–6190 (1997).
- Tomić, S. *et al.* Screening and fundamental length scales in semidilute Na-DNA aqueous solutions. *Phys. Rev. Lett.* **97**, 098303 (2006).
- Robinson, R. A. & Stokes, R. H. *Electrolyte Solutions* (Butterworths, London, 1959).
- Lindsay, S. M. *et al.* The origin of A to B transition in DNA fibers and films. *Biopolymers* **27**, 1015–1043 (1988).
- Besteman, K., Van Eijk, K. & Lemay, S. G. Charge inversion accompanies DNA condensation by multivalent ions. *Nature Phys.* **3**, 641–644 (2007).



54. Lee, D. J., Wynveen, A., Kornyshev, A. A. & Leikin, S. Undulations enhance the effect of helical structure on DNA interactions. *J Phys. Chem. B* **114**, 11668–11680 (2010).

Acknowledgments

This research was supported by the U.S. Department of Energy, Office of Basic Energy Sciences, Division of Materials Sciences and Engineering under Award DE-SC0008176.

Author contributions

S.Y., R.P. and V.A.P. designed research; S.Y., R.P. and J.V.O. performed research; J.V.O. and M.J. contributed new reagents and tools; S.Y., R.P. and V.A.P. analyzed data; S.Y. prepared figures; and S.Y. and R.P. wrote the paper. All authors reviewed the manuscript.

Additional information

Supplementary information accompanies this paper at <http://www.nature.com/scientificreports>

Competing financial interests: The authors declare no competing financial interests.

How to cite this article: Yasar, S., Podgornik, R., Valle-Orero, J., Johnson, M.R. & Parsegian, V.A. Continuity of states between the cholesteric \rightarrow line hexatic transition and the condensation transition in DNA solutions. *Sci. Rep.* **4**, 6877; DOI:10.1038/srep06877 (2014).



This work is licensed under a Creative Commons Attribution-NonCommercial-NoDerivs 4.0 International License. The images or other third party material in this article are included in the article's Creative Commons license, unless indicated otherwise in the credit line; if the material is not included under the Creative Commons license, users will need to obtain permission from the license holder in order to reproduce the material. To view a copy of this license, visit <http://creativecommons.org/licenses/by-nc-nd/4.0/>